Microstructure of Weld Heat-Affected Zone in Cold Rolled Aluminum Plate†

Toshio ENJYO * and Saburo NASU **

Abstract

Hardness and tensile strength measurements of cold rolled aluminum plate (A1080) after MIG welding procedure using a filler metal (A1100W) were re-examined as a function of the initial rolling reduction of thickness from 5% to 63%, and then the direct observations of microstructures at heat-affected zone (HAZ) have been performed using a technique of thin foil transmission electron microscopy. Compression texture of the base metal changes to the annealing texture at HAZ and the deformed region at high temperature as a formation of dislocation cell structure and tangled dense dislocations could be observed at the near of fusion line between deposited weld metal and heat-affected zone (HAZ). In deposited weld metal, the impurity segragation at grain boundaries is quite appreciable compared in HAZ and the results from electron-probe X-ray microanalysis have been discussed briefly.

1. Introduction

It is well recognized that the various properties, especially for mechanical properties, of weld joints in aluminum and its alloys depend on the properties of heat-affected zone as well as that of deposited weld metal. Heat-treatments at heat-affected zone induced by the weld thermal cycle include relatively short-time heating and cooling in which various peak temperatures are distributed in the range from room temperature to just below the melting point of base metal. It is quite acceptable that the heat-treatments by weld thermal cycle should be largely differ from the usual heat--treatments as isothermal annealing. Principally at the heat-affected zone in cold rolled pure aluminum it can be observed the change from deformed states to annealed one.

Namba, Fukui and Sugiyama[1] have reported the recrystallization behaviour at heat-affected zone of welded commercially pure aluminum (A1100) in connection with their effects on the tensile strength. They measured the width of recrystallized zone and grain size at the heat-affected zone (HAZ). Softenning at HAZ was found in accordance with ordinary recrystallization sequence, but the extraordinary grain growth as a secondary recrystallization was not observed. More microscopic investigation including the discussions about the rearrangements of dislocation sub-structures and the formation of sub-boundaries will be quite important for the better understanding on recrystallization behavior at HAZ. Utilizing thin foil transmission electron microscopy, it becomes possible to study more microscopic structure at weld heat-affected zone (HAZ) in cold rolled aluminum plate. Direct observations of the dislocation sub-structure and the formation of sub-boundaries are possible only with a aid of the technique of thin foil transmission electron microscopy.

In this investigation, hardness and tensile strength measurements of cold rolled aluminum plate (A1080) after MIG welding procedure were re-examined as a function of the initial rolling reduction of thickness and then direct observations of microstructure at heat-affected zone (HAZ) were performed using thin foil specimens. Compression texture of the base metal changes to the annealing texture at HAZ and the deformed region at high temperatures could be observed at the near of fusion line between deposited weld metal and heat-affected zone (HAZ). In deposited weld metal, the impurity segragation at the grain boundary is observed and the electron-probe X-ray microanalysis clarified the differences in distribution of iron and silicon impurities between HAZ and the deposited weld metal.

† Received on July 26, 1975

* Professor

** Research Instructor

2. Experimental Details

Chemical compositions of materials used as a base metal (A1080) and a filler metal (A1100W) are shown in Table 1. It should be noted that the contents of iron

Table 1. Chemical Compositions (wt.%)

	Cu	Si	Fe	Mn	Mg	Zn	Cr	Ti	Al
A 1080	0.01	0.06	0.11	<0.001	<0.001	0.01	<0.001	<0.001	Bal.
A 1100W	0.05	0.17	0.48	0.02	0.01	0.01	<0.001	0.016	Bal.

and silicon impurities in filler metal (A1100W) are larger than those of the base metal (A1080). This fact affected probably on the difference in the morphology and distribution of these impurities between deposited weld metal and base metal as discussed in Section 3.3.

Platellet specimens whose thickness are from 16 mm to 6.5 mm were firstly annealed for 1 hour at 300°C and then cold rolled up to the constant thickness of 6 mm in order to get various resultant thickness reductions from 5% to 65%. A1100W wire as filler metal was 1.6 mm in diameter. Bead-on-plate weldings were performed with MIG. The welding conditions were as follows; welding current, 230A, arc voltage, 24V, and welding speed, 60 cm/min.

Rectangular specimens whose center positions are just as weld joints were used for tensile strength tests by Instron type machine, Vicker's hardness tests and observations of the macrostructures by optical microscopy. Size of these rectangular specimens was as follows; width, 20 ~ 25 mm, length, 80 mm and thickness, 6 mm. For the observations by thin foil electron microscopy, the plate of about 1 mm in thickness were cut out from this rectangular specimen and the positions to cut are shown as I, II, III and IV in Photo. 1. These 1 mm thick platellet specimens were fixed at the bottom of specially designed jig using a glycophthalate wax and a mechanical thinning was performed in water up to 0.1 ~ 0.3 mm in thickness. After mechanical thinning these strips are electropolished by jet technique in a electrolyte (ethyl-alcohol, 90% and perchloric acid, 10%) at about 10°C. Specimens are examined at room temperature using Hitachi type HU-12A electron microscopy. Operations are always performed at accelation voltage 100 KV. Electron-probe X-ray microanalysis are performed by Shimazu type EMX-1A analyzer. Accelation voltage was 25 KV and the electron beam-spot has a size of about 5 micron in diameter.

3. Experimental Results and Discussions

3.1. Hardness and tensil strength tests

Figure 1 shows the typical macrostructure and the distribution of Vicker's hardness number obtained from

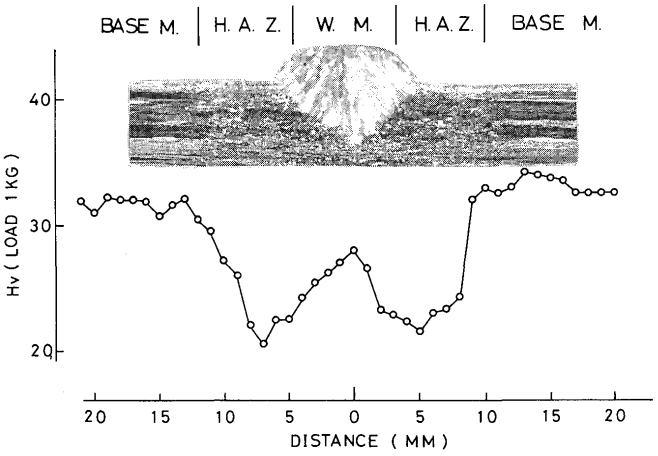

Fig. 1 Typical macrostructure of the weld joints and the distribution of Vicker's hardness number as a function of distance from the center of deposited weld metal. Specimen was cold rolled initially up to 63% reduction in thickness.

the specimen which was cold rolled up to 63% reduction in thickness and welded with MIG. Fiber structures induced by the compression of cold rolling are clearly shown at non-affected zone. Recrystallization behavior characterized by the vanishing of fiber structure can be observed as a formation of the heat-affected zone (HAZ) and the appreciable drop in Vicker's hardness number is found in this region, HAZ. However, the extraordinary grain growth as a secondary recrystallization could not find macroscopically even near the fusion line where the temperature was high and rised up to just below the melting point. At deposited weld metal the increase of Vicker's hardness number was found. In connection with this increase we examined the distribution of iron and silicon impurities in this region using a electron-probe X-ray microanalysis and the results obtained were discussed briefly in Section 3.3.

Softenning at HAZ could be found and the width of HAZ deduced from the hardness measurements are shown in Fig. 2 as a function of the initial thickness reduction. Minimum and maximum values of the width for softened HAZ, which were denoted by W_L and W_H respectively in Fig. 2, did not depend on the magnitude of initial thickness reduction.

Figure 3 and 4 show the dependence of the hardness number and the maximum tensile strength on

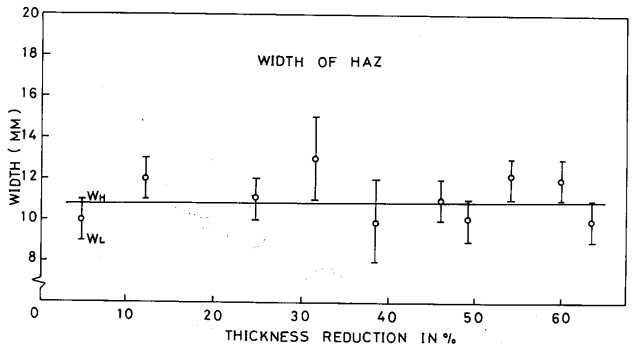

Fig. 2 Width of the softenned region near weld joints, namely heat-affected zone (HAZ), as a function of initial reduction in thickness. W_L and W_H indicate the minimum and maximum values for the width of HAZ.

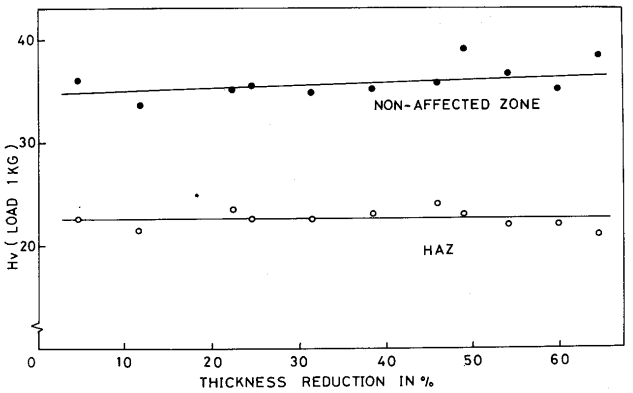

Fig. 3 Vicker's hardness number for base metal, namely for non-affected zone, and for HAZ as a fuction of initial thickness reduction.

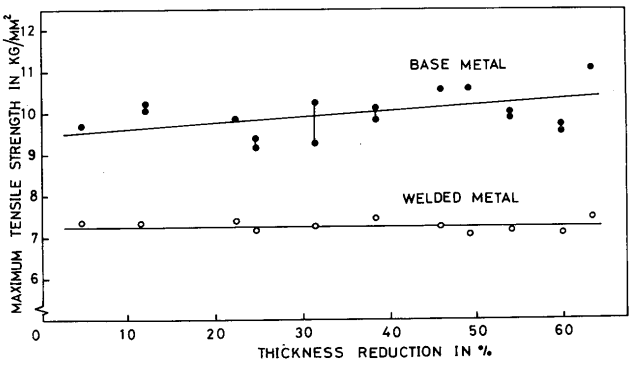

Fig. 4 Dependence of the maximum tensile strength of base metal and welded metal as a function of initial thickness reduction.

the magnitude of initial thickness reduction. For base metals, both values depend on the thickness reduction. However the specimens containing weld joints did not show any dependence on the magnitude of the thickness reduction. From these results we can say that pure aluminum A1080 which was welded with MIG does not show the dependence of hardness and maximum tensile strength on the initial thickness reduction of base metal and does not agree with the results previously reported for A1100 aluminum[1]. Reasonable explanations about this disagreement may be contain the difference on the contents of impurities such as iron and silicon when comparison was performed between A1080 and A1100 aluminum.

3.2. Electron microscopic obervations

Positions, from which platellet specimens were cut out and the electron microscopic observations were performed after thinning procedures, are shown in Photo. 1 as I, II, III and IV. A, B and C show the positions near the fusion line in specimen IV. D and E show the positions in deposited weld metal. In all specimens the foil planes are parallel to the direction of weld bead.

Photograph 2 shows the thin foil electron micrograph obtained from the specimen I. Initially base metal

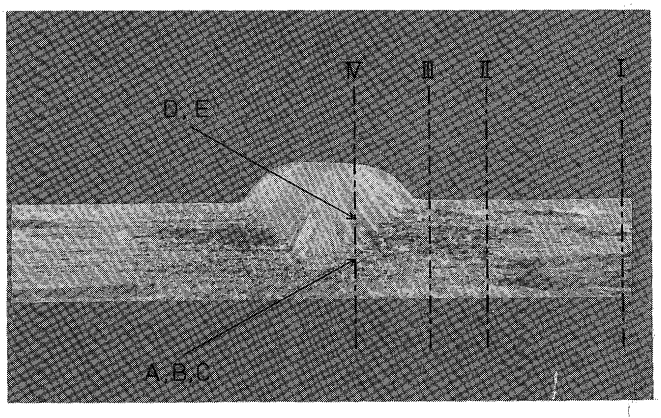

Photo 1 Macrostructure and the positions for transmission electron microscopic observations. A, B and C are the regions near fusion line. D and E are the regions in deposited weld metal.

was cold rolled and the thickness reduction was 63%. Deformation structures are clearly shown in this photograph. In Photo. 2 (a) tangled dislocations and tilted boundary are shown. In Photo. 2 (b) transition bands which were introduced by cold rolling, namely the compressive deformation, are shown as perpendicular to the compression axis. Wall of the transition band was indicated as arrow in Photo. 2 (b). Photograph 2 (c) shows the distributions of dislocations and high dense dislocations may be come loose during the thinning procedure. Photograph 2 consequently shows the deformed structure in non-affected zone which contains the tilted high energy grain boundaries, tangled dislocations and the transition bands elongated by the compression.

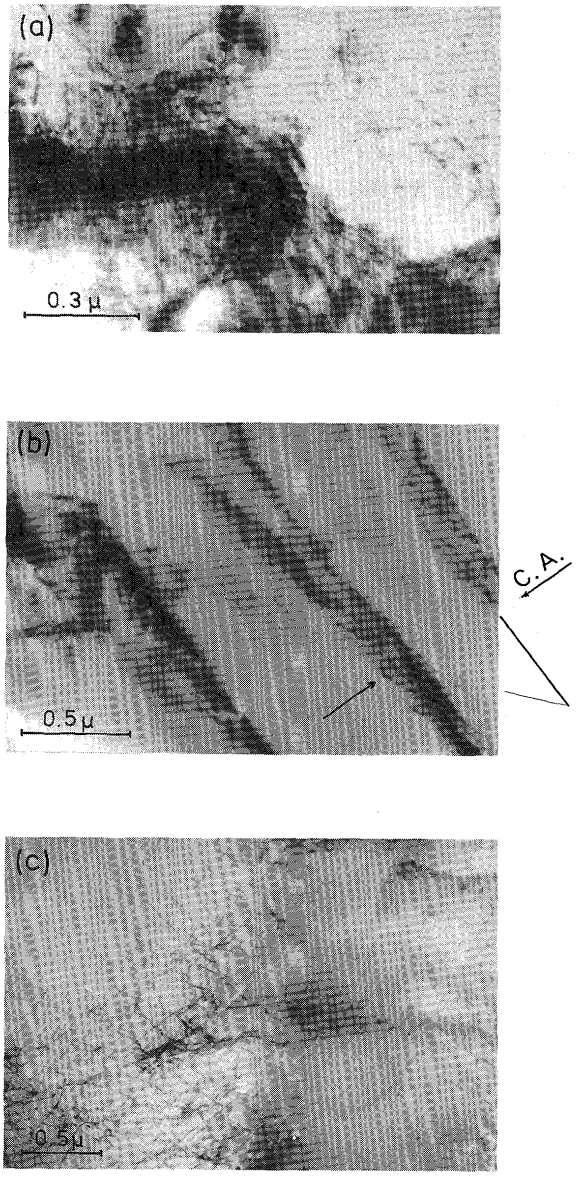

Photo 2 Electron micrographs obtained from the postion I of photo 1, namely from the non-affected zone. Base metal was cold rolled initially up to 63% reduction in thickness.
(a) Tangled dislocaitons and tilted boundary, (b) Transition band and its wall is perpendicular to the compression axis, (c) Relatively low density of the dislocations suggests that thinning procedure makes to come loose high dense dislocations.

Photograph 3 shows the electron diffraction pattern and its analysis obtained from the position I, but the thin foil specimen has a perpendicular orientation to the compression axis. Diffraction pattern indicates the specimen foil is nearly {110} planes and the electron-beam enters parallel to the [110] direction mostly. Since the foil plane is perpendicular to the compression axis, the compression axis is nearly parallel to the [110] direction and the foil plane indicates the [110] compression texture. For aluminum the [110] compression texture is observed[2] and the wall of the transition band which was indicated in photo. 2 (b) is parallel to nearly {110} planes.

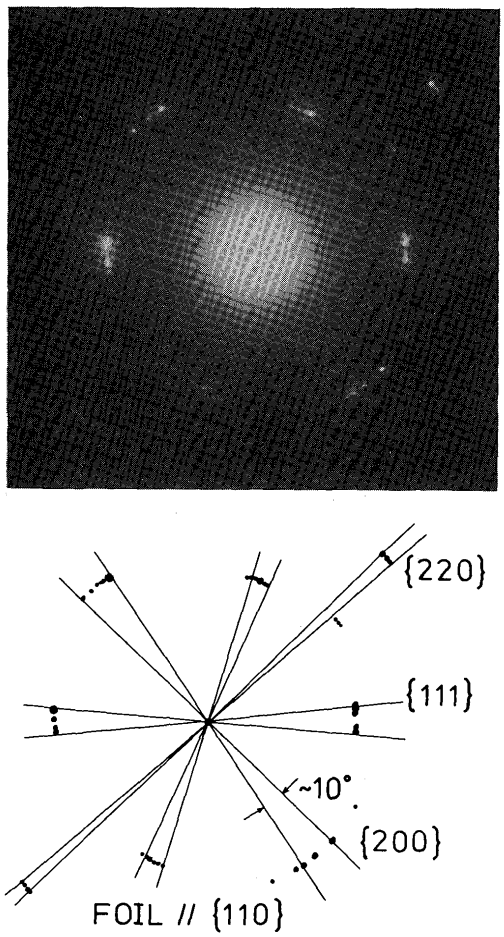

Photo 3 Electron diffraction pattern and index of spots obtained from the same position I of photo 1, as shown in photo 2. But the foil plane is nearly perpendicular to the compression axis.

Photograph 4 shows the micrograph obtained from the specimen II. In Photo. 4 (a) many sub-boundaries are formed within the transition bands and the wall of transition bands tends to form the stable high angle grain boundary. Arrows and the notation of C. A. indicate the initial wall of transition band and the direction of compression axis, because the transition bands elongated by cold rolling perpendiculary to the compression axis. In Photo. 4 (b) a stable high angle grain boundary and the cross point of sub-boundaries are seen and it is clear that the regular array of boundary dislocations exists and the tilt angles between these sub-boundaries are not so large. In Photo. 4 (c) the small angle grain boundary indicated as a single array of

dislocations could be observed and sparse dislocations were also observed in matrix. From this Photo. 4 it is clear that in this region of HAZ far from the deposited weld metal recrystallization behavior occurred as the formation of sub-boundaries within the transition bands. Since the transition band was induced by the cold rolling and perpendicular to the compression axis, the formation of sub-boundaries within the transition bands suggests the change of [110] compression texture.

Photograph 5 indicates the diffraction pattern and

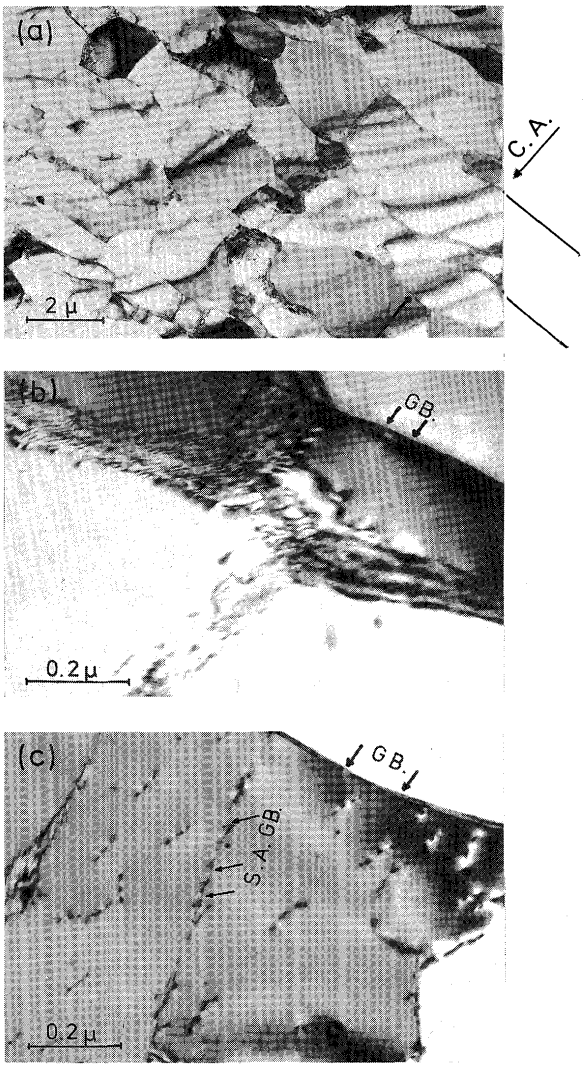

Photo 4 Electron micrographs obtained from the positon II of photo 1, namely from HAZ. (a) Many sub-boundaries within the transition bands with relation to the compression axis (C.A.). (b) Stable grain boundary (G.B.) and sub-boundaries which were formed by the array of boundary dislocations. (c) Stable grain boundary (G.B.) and the small angle grain boundary (S. A. GB.) of single array of boundary dislocatins. Within the grain, the dislocations exist sparsely.

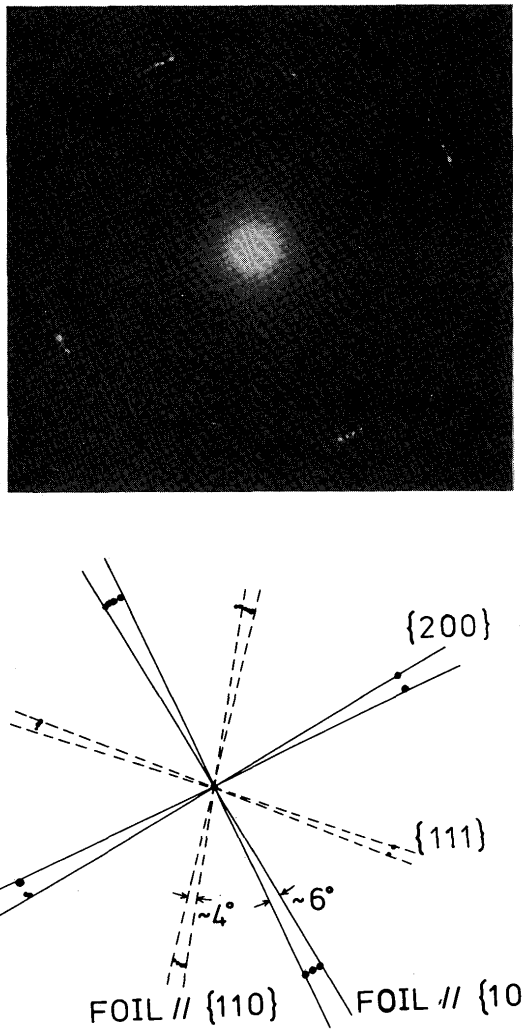

Photo 5 Electron diffraction pattern and index of spots obtained from the same position II of photo 1, as shown in photo 4. But the foil plane is nearly perpendicular to the compression axis.

the schematic analysis of diffraction spots. Electron-beam was perpendicular to the specimen foil and its direction indicates [100]. From this fact the matrix [110] direction changed to the [100] direction at HAZ and the sub-boundary formations within transition bands were deduced as a consequence of the formation of {100} annealing texture. Intensity of {200} spots in Photo. 5 is stronger than that of {111} spots and suggested that the probability to find {100} planes within the specimen foil is larger than that of {110} planes.

Photograph 6 shows the electron micrograph obtained from same position as specimen II but the initial thickness reduction was only 5%. Clear transition bands induced by compressive deformation could not be

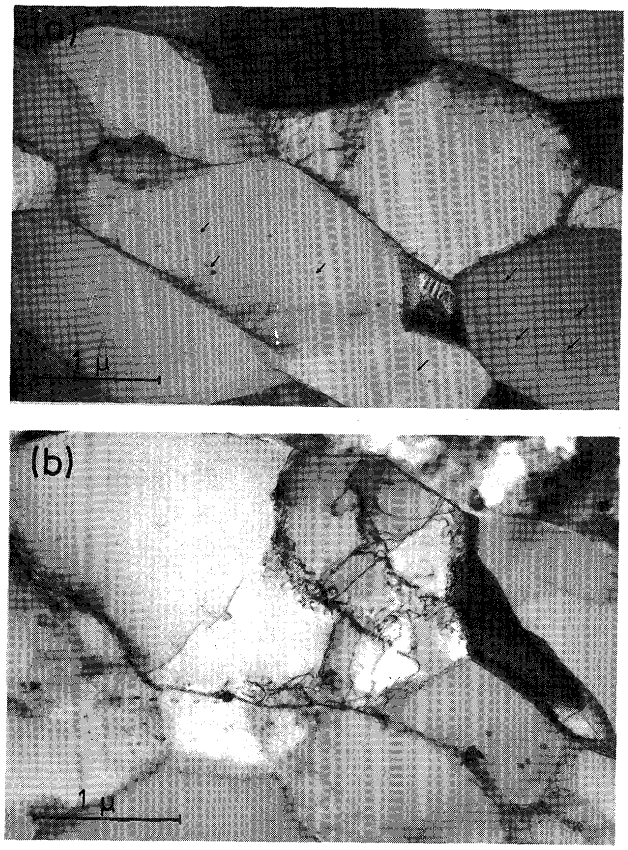

Photo 6 Electron micrographs obtained from the position II of photo 1, namely from HAZ, but the initial thickness reduction was only 5%. Arrows in (a) indicate the regular array of the precipitates and/or segregations of impurities.

observed and the sub-boundaries were stable. It is observed that the regular array of precipitates and/or segragations by impurities exist in matrix. This fact indicates that the migration of sub-boundaries occured during the weld thermal cycle at HAZ for the specimen slightly deformed as 5% thickness reduction. This type of recrystallization behavior is differ from that of 65% thickness reduction specimen, because the formation of sub-boundaries is only occured within the transition bands and the migration of boundaries is not appreciable for the specimen cold rolled heavily.

Photograph 7 shows the electron micrograph obtained from the specimen III which deformed initially up to 65% thickness reduction. Very stable grain boundary which indicates nealy 120 degree of angles at a cross point was found and the relatively straight dislocations are also observed in matrix. Consequently the existence of low density of dislocations can be predicted in this region of HAZ, after the offering of the weld thermal cycle.

However quite high density of the dislocations induced by the high temperature deformation are observed at very near to the fusion line and discussed as below. Photograph 8 A indicates similar structure resulted from the creep deformation at high temperature, namely

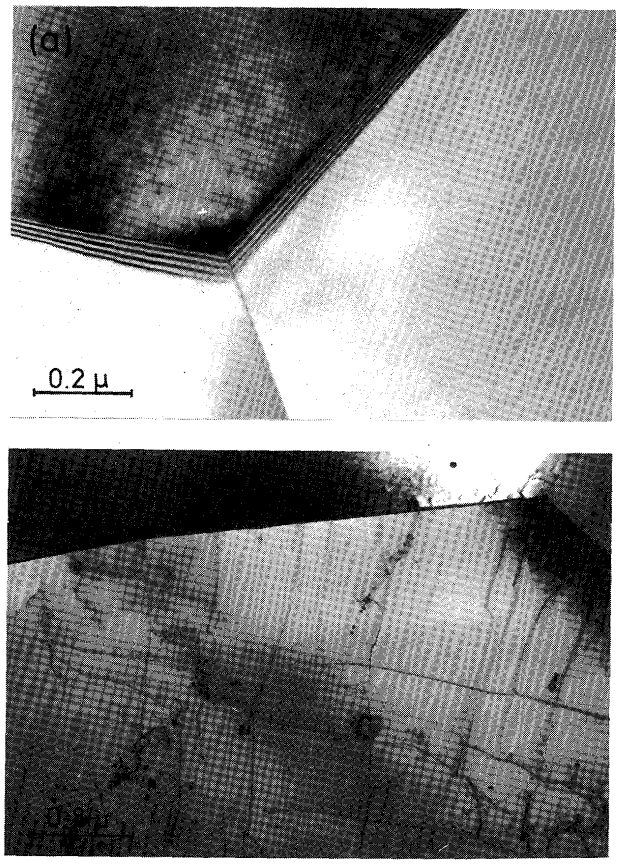

Photo 7 Electron micrographs obtained from the position III of photo 1, namely from inner parts of HAZ. (a) Very stable grain boundaries crossed by the angle of nearly 120 degree. (b) Loose and straight dislocations.

dislocation cell structure. According to the Ball's investigation[3], the tensile flow stress being supplied to the specimen has a well described relation with the cell size formed by the deformation and the relation is given by

$$\text{Tensile flow stress } \sigma = k \cdot t^{-1/2}$$

where k is proportionality constant and t is observed cell size. From this relation the local tensil flow stress in this region was deduced to be about 5 Kg/mm^2. In Photo. 8, B indicates the tangled and high dense dislocations and C shows the micrograph in which the cell boundary coincides to the foil plane. Reasonable explanation for the existence of deformed region near fusion line may be due to the volume change at the deposited weld metal by the solidification. Existence of the deformed region near fusion line is quite interesting because this region is quite important for the properties of weld joints such as chemical and mechanical properties.

Photograph 9 shows the electron micrograph obtained from the regions of D and E in specimen IV. D and E regions indicate the deposited weld metal. Morphology of the sub-boundaries in Photo. 9 is differ from that of some regions in HAZ. Most appreciable feature of the microstructure in deposited weld metal is the impurity segragation on the boundaries which were indicated as arrows in Photo. 9. For the explanation for the existence of this segragation, we must consider the difference of impurity contents between base metal and filler one. However the solidification speed which is relatively high at welding procedure is also very important when the iron impurity is the main term in a segragation and/or precipitation phenomena[4].

From above electron microscopic observations including some electron diffraction analysis, the recrystallization behaviors at HAZ are summarized as follows and schematic illustration for the results obtained is shown in Fig. 5. (1) Initially [110] compression texture of base metal changes to the [100] annealing texture at HAZ. For the specimen cold rolled heavily, the sub-boundary formation was occured within the transition band. (2) At the center of HAZ, sub-boundary migration was occured and the formation of stable boundary exists. Probably the range of these regions depends on the initial thickness reduction, but detailed discussion needs more precise observations. However the well known mechanism for the secondary recrystallization, that is the nucleation and growth of the selective grain, could not be observed even in this region. (3) At near the fusion line, deformed regions are observed and it was deduced that the high temperature deformation was occured at this region.

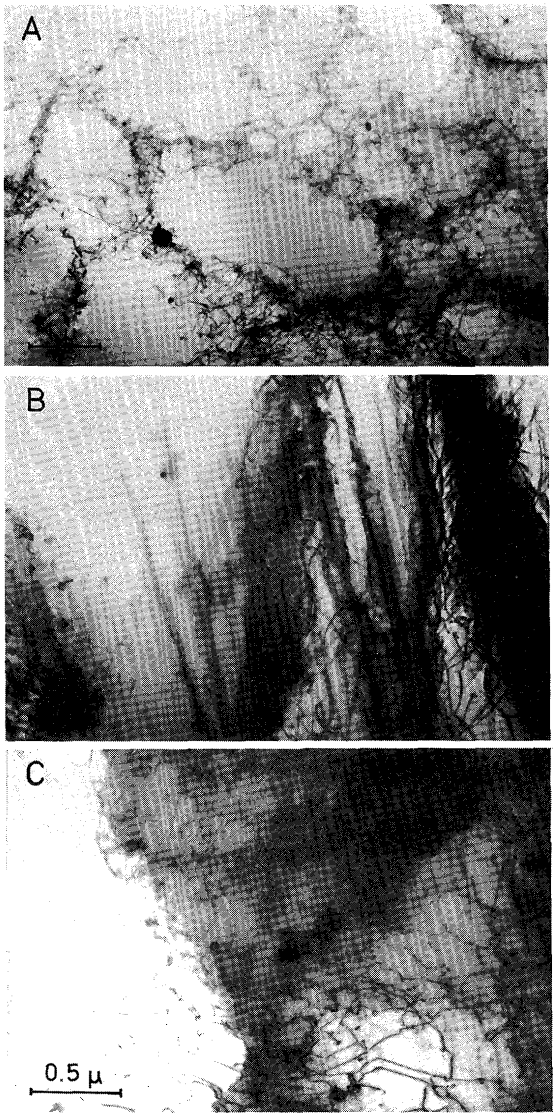

Photo 8 Electron micrographs obtained from the regions denoted as A, B and C in the position IV of photo 1. A; dislocaiton cell structure and the averaged local tensile flow stress was deduced by the averaged cell size in text. B; tangled dislocations. C; cell boundary located on the foil plane.

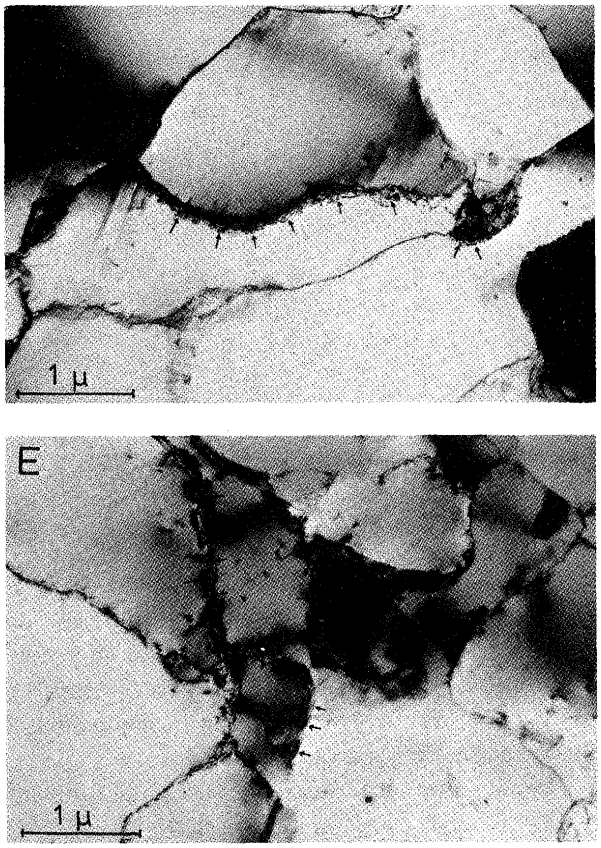

Photo 9 Electron micrographs obtained from the regions denoted as D and E in the position IV of photo 1, namely from the deposited weld metal. Arrows in D and E are complex contrasts arized from the impurity segragations in boundaries.

3.3 On the distribution of Fe and Si impurities

At previous sections, the large values in Vicker's hardness number and the appreciable segragation of the impurity at grain boundaries were found in deposited

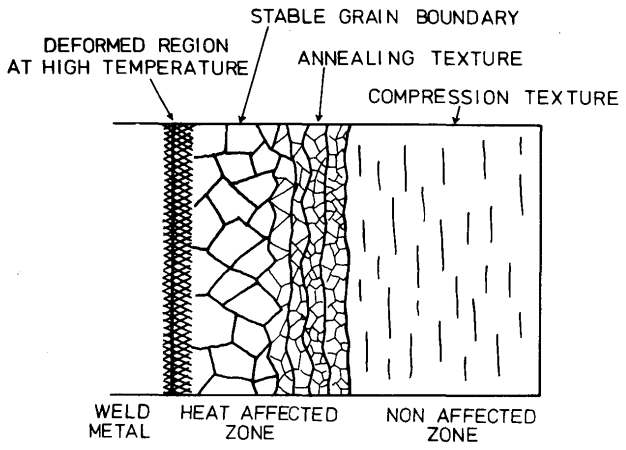

Fig. 5 Schematic illustration for the recrystallization behavoir at HAZ.

weld metal but not in HAZ. In commercially pure aluminum, it is well recognized that iron and silicon impurities are always contained and quite important for its properties because of the extremely small solid solubility of iron and its formation of compounds with silicon and/or its segragations[5~7].

Results from the electron-probe X-ray scanning of Fe K_α and Si K_α lines are shown in Fig. 6 and 7. Large difference was observed between deposited weld metal and HAZ. At HAZ the Si intensity was detected largely, but the Fe line is not so dense. However at the region of deposited weld metal the Si line could not be observed and the Fe line was quite dense. From this

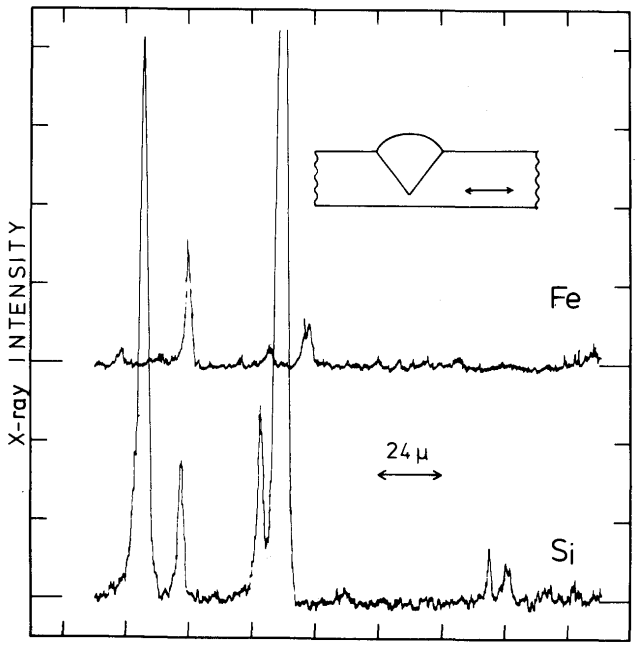

Fig. 6 Electron-probe X-ray scanning by Fe K_α and Si K_α radiations in HAZ. Scanning position was shown as arrow in the figure.

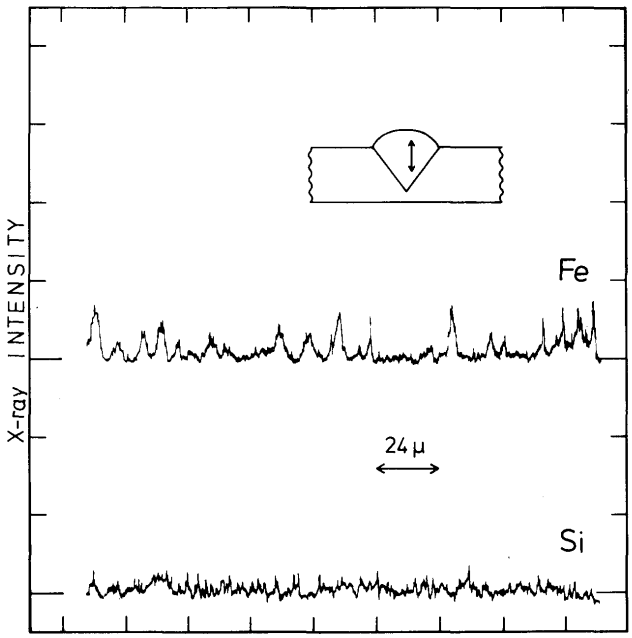

Fig. 7 Electron-prove X-ray scanning by Fe K_α and Si K_α radiations in deposited weld metal. Scanning position was shown as arrow in the figure.

results we can deduced that the Al-Fe binary compounds are finely dispersed in deposited weld metal, but at HAZ Al-Fe-Si ternary compounds and the Si particles may be exist.

4. Conclusive Remarks

Hardness and tensile strength measurements of cold rolled aluminum plate (A1080) were examined after MIG welding procedure. Direct observations of microstructure at heat-affected zone (HAZ) were performed using a technique of thin foil transmission electron microscopy. Specimens containing weld joints did not show any dependence for their magnitude of the HAZ width, Vicker's hardness number and the maximum tensile strength on the magnitude of initial thickness reduction of base metal, though the each base metal depends for its mechanical properties on the magnitude of the initial thickness reduction. Direct observations of thin foil specimens at non-affected zone, some parts at HAZ and deposited weld metal suggest following results: (1) [110] compression texture at non-affected zone changes to the [100] annealing texture at HAZ. (2) Sub-boundary migrations and formation of stable boundaries were occured in the center region at HAZ, but the apparent secondary recrystallization could not be observed. (3) Deformed regions as a formation of dislocation cell structure and tangled dense dislocations are observed near the fusion boundary and suggested that the

some kinds of deformation were occured during and/or after welding procedure. (4) Finally the appreciable impurity segregation was observed in the deposited weld metal. Electron-probe X-ray microanalysis was performed in order to compare the morphology and distribution of iron and silicon impurities in deposited weld metal and HAZ, and found the difference in distribution of these impurities.

Acknowledgements

The authors wish to thank Mr. T. Horinouchi for his variable contributions in this work. The support of the Light Metal Educational Foundation is grately acknowledged.

References

1) K. Namba, T. Fukui and Y. Sugiyama; "On the Recrystallization Behavior at Weld Heat-affected-zone of Commercially pure Aluminum," J. Japan Weld Soc., Vol. 43 (1974) p.3.
2) C. S. Barrett; "Structure of Metals," McGraw-Hill Book Co., (1952). R. W. Cahn; "Recovery and Recrystallization," in Physical Metallurgy, edited by R. W. Cahn, North-Holland, (1965) p.925.
3) C. J. Ball; "The Flow Stress of Polycrystalline Aluminum," Phil. Mag., Vol. 7 (1957) p.1011.
4) E. H. Hollingsworth, G. R. Frank Jr. and E. E. Willet; "Identification of a New Al-Fe Constituent, $FeAl_6$," Trans. AIME, Vol. 224 (1962) p.188.
5) Y. Murakami, S. Nasu, S. Sugiyama, K. Kawabe, T. Onishi and T. Kishimoto; "Study on Intermetallic Compounds in a Commercially pure Aluminum-ingot," Light Metal, Vol. 23 (1973) p.492.
6) J. K. Edgar; "Solid Solubility of Fe in Al," Trans. AIME, Vol. 180 (1949) p.225.
7) M. Nishio, S. Nasu and Y. Murakami; "Solid Solubility of Iron in Aluminum by means of the Fe^{57} Mössbauer Effect", J. Japan Inst. Metals, Vol. 34 (1970) p.1173.